doi.org/10.36721/PJPS.2026.39.7.192.1

Lactate related metabolic reprogramming increases global protein lactylation and remodels tumor immune microenvironment of hepatocellular carcinoma

Taiyu Xia[1#], Ya Li[1#], Xuemei Zhao[1]* and Zhengwei Song[2]*

[1]Department of Oncology, Dazu Hospital of Chongqing Medical University, The People's Hospital of Dazu, Chongqing, China.
[2]Department of Hepatobiliary Surgery, Dazu Hospital of Chongqing Medical University, The People's Hospital of Dazu, Chongqing, China.

Abstract: **Background**: Hepatocellular carcinoma (HCC) is characterized by profound metabolic reprogramming and an immunosuppressive tumor immune microenvironment (TIME). Lactate accumulation has recently been implicated in protein lactylation and tumor progression, but its role in reshaping the TIME in HCC remains incompletely understood. **Objectives**: To investigate how lactate-related metabolic reprogramming influences global protein lactylation and the TIME in HCC. **Methods**: We integrated high-throughput RNA sequencing, construction of a lactate metabolic process activity (LMPA) model, molecular subtyping, survival analysis and single-cell RNA sequencing to characterize lactate-associated alterations in HCC. Tissue microarrays and in vitro functional assays were used to validate key findings. **Results**: Elevated expression of lactate dehydrogenase A (LDHA), a core enzyme in lactate metabolism, was significantly associated with altered transcriptional profiles, unfavorable survival and changes in TIME composition in patients with HCC. In vitro, LDHA overexpression promoted HCC cell proliferation, migration and invasion. Patients with high LMPA exhibited significantly poorer prognosis and distinct immune infiltration patterns, including altered proportions of B cells, CD4+ T cells, neutrophils, macrophages, and dendritic cells. Single-cell RNA sequencing further revealed heterogeneous LMPA patterns across cell populations and increased global protein lactylation, particularly in immune cells. In addition, LMPA-based molecular subtypes were closely associated with lactylation-related features. LDHA expression, HDAC2 expression and metastasis were identified as significant prognostic factors. **Conclusion**: Lactate-related metabolic reprogramming may enhance global protein lactylation and remodel the TIME in HCC, thereby promoting tumor progression. These findings highlight the potential of targeting lactate metabolism and lactylation-associated pathways as novel therapeutic strategies for HCC.

Keywords: Hepatocellular carcinomas; Metabolic reprogramming; Lactates; Tumor microenvironments

Submitted on 07-11-2024 – Revised on 13-07-2025 – Accepted on 28-07-2025

INTRODUCTION

Hepatocellular carcinoma (HCC) is a highly prevalent and lethal malignancy, ranking among the leading causes of cancer-related death both worldwide and in China (Xia *et al*., 2022). Despite the development of various treatment strategies, the prognosis for patients with HCC remains unsatisfactory due to its aggressive biological behavior, high recurrence rate and resistance to conventional therapies (Chen *et al*., 2020; Harding-Theobald *et al*., 2021; Wang and Wei, 2020).

In recent years, the tumor immune microenvironment (TIME) has gained increasing attention as a critical factor influencing HCC progression and treatment response (Lu *et al*., 2019; Oura *et al*., 2021). Various TIME-targeted therapeutic approaches, including immune checkpoint inhibitors, have shown encouraging results in some patients, yet overall clinical benefits remain limited (Sheng *et al*., 2020; Xu *et al*., 2018). One of the key reasons is that the TIME in HCC is often immunosuppressive and dynamically regulated by tumor metabolic pathways (Giannone *et al*., 2020).

Among these pathways, lactate metabolism has been recognized as a central component of tumor metabolic reprogramming (Chen *et al*., 2025; Nguyen *et al*., 2025), especially in HCC (Pedretti *et al*., 2025). Aberrant lactate production and accumulation can reshape the TIME by affecting immune cell function and promoting an immunosuppressive environment (Llibre *et al*., 2025). Recent evidence suggests that histone lactylation can be catalyzed by enzymes such as p300, which functions as a lactyltransferase, while histone deacetylases (HDACs) can modulate its removal (Deng *et al*., 2025; Zhang and Zhang, 2024). Accumulated lactate may enhance these modifications, leading to widespread transcriptional reprogramming in tumor and immune cells. However, the specific role of lactate metabolism, including its associated lactylation modifications, in modulating the TIME of HCC remains incompletely understood.

A deeper understanding of how lactate-related metabolic reprogramming interacts with the TIME may provide new insights into HCC progression and offer potential avenues for more effective therapeutic strategies.

**Corresponding author:* e-mail: szwei19841021@163.com
#These authors contributed equally and are the co-first authors.

MATERIALS AND METHODS

Cell culture and gene editing

HepG2 cells were obtained from Procell (Cat. No.: CL-0103; RRID: CVCL_0027). Huh7 cells were obtained from Procell (Cat. No.: CL-0120; RRID: CVCL_0336). HepG2 and Huh7 cells were maintained in DMEM supplemented with fetal bovine serum (FBS). When the cells reached approximately 75% confluence, they were seeded into 6-well plates and transfected using Lipofectamine 3000 according to the manufacturer's instructions. The culture medium was replaced 6-8 hours after transfection and cells were harvested after 48 hours. The experimental groups included NC (negative control siRNA), si-LDHA (LDHA-targeting siRNA), vector (empty vector plasmid) and OE-LDHA (LDHA overexpression plasmid). The transfected cells were then used for subsequent functional assays.

CCK-8 proliferation assay

HepG2 or Huh7 cells of each group were seeded in 96-well plates with three replicate wells per group. Cells were allowed to adhere overnight, then cultured for 24, 48, 72 and 96 hours to assess proliferation. CCK-8 reagent (10 μL) was added to each well, mixed gently and incubated in the dark for 3 hours. Absorbance at 450 nm (Cai *et al*., 2024) was then measured using a SpectraMax i3x microplate reader (Molecular Devices, San Jose, CA, USA). Mean OD values for each group were calculated after subtracting blank well values.

EdU assay

HepG2 or Huh7 cells from each group were seeded onto chamber slides. After allowing the cells to adhere, the EdU labeling medium was added and the cells were incubated for 3 hours. The cells were fixed and EdU incorporation was detected using fluorescent reaction solution according to the kit instructions. EdU-positive cells were visualized under a fluorescence microscope (Olympus Corporation, Tokyo, Japan) and the percentage of EdU-positive cells was calculated to assess cell proliferation.

Transwell assay

A total of 100 μL of Matrigel was added to 24-well Transwell inserts and allowed to solidify at 37 °C. Then, 100 μL of a cell suspension from each HepG2 or Huh7 group was seeded into the upper chamber, while the lower chamber was filled with culture medium supplemented with FBS. After 24 hours of incubation, the inserts were washed, stained and the number of invading cells was counted under an Olympus BX53 light microscope (Olympus Corporation, Tokyo, Japan).

Wound healing assay

HepG2 or Huh7 cells from each group were seeded into 6-well plates. When the cells reached confluence, a linear scratch was created using a sterile pipette tip. The wells were gently washed to remove detached cells and then incubated for 24 hours. After incubation, the cells were rinsed and imaged under an Olympus BX53 light microscope (Olympus Corporation, Tokyo, Japan). The number of cells that migrated into the wound area was quantified to assess cell migration ability.

Data acquisition

RNA-seq data and clinical information for HCC samples were obtained from The Cancer Genome Atlas (TCGA) and International Cancer Genome Consortium (ICGC), with count data normalized to TPM and transformed using log2(TPM+1). Additionally, GSE140228 and GSE149614 datasets were retrieved from Gene Expression Omnibus (GEO) for further analysis.

Gene sets

The lactate metabolic process gene set was obtained from Gene Ontology and downloaded from the Molecular Signatures Database (Liberzon *et al.,* 2015).

Differential expression analysis

The R package limma was used to identify differentially expressed genes, applying thresholds of adjusted p-value < 0.05 and |log2(fold change)| > 1.

Enrichment analysis

Enrichment analysis was conducted to explore the functions of differentially expressed genes. Gene Ontology (GO) annotations categorized genes into molecular function (MF), biological process (BP) and cellular component (CC). Kyoto Encyclopedia of Genes and Genomes (KEGG) analysis provided insights into functional pathways. The R ClusterProfiler package (v3.18.0) (Yu *et al*., 2012) was used for GO and KEGG analyses, while ggplot2 and pheatmap were used to create boxplots and heatmaps, respectively.

Analysis of TIME composition

To obtain a reliable immune score assessment, the xCell and TIMER algorithms from the R immuneeconv package were used (Aran *et al*., 2017; Li *et al*., 2020), both of which are benchmarked with unique advantages. Expression of immune checkpoint genes was extracted.

Construction of LMPA model

The log-rank test compared survival differences between groups. The timeROC package (Blanche *et al*., 2013) assessed predictive accuracy. Multivariate Cox regression constructed a prognostic model using the survival package. Stepwise iteration selected the optimal model.

Molecular subtyping

Consensus unsupervised clustering was performed using the ConsensusClusterPlus R package (Wilkerson and Hayes, 2010), clustering samples into 2-6 subgroups with 80% resampling over 100 iterations using hierarchical clustering (clusterAlg = 'hc', innerLinkage = 'ward.D2'). Heatmaps were generated by pheatmap.

Analysis of single-cell RNA-seq data

Single-cell RNA-seq datasets (GSE140228 and GSE149614) were downloaded from the GEO database. After initial quality control, cells with high mitochondrial

gene expression or low unique gene counts were excluded to remove low-quality cells. In total, 6582 cells for GSE140228 and 15493 cells for GSE149614 were retained for downstream analysis. All samples were renamed, merged and imported into R (v4.2.2) using the Seurat package (v5.0.3). Batch effects among samples were corrected using the Harmony algorithm. The data were then normalized, scaled and the top variable genes were identified for dimensionality reduction by principal component analysis (PCA) and visualized by uniform manifold approximation and projection (UMAP). To assess lactate metabolic process activity (LMPA) at the single-cell level, AUCell was used to calculate enrichment scores for each cell. For trajectory inference, pseudotime analysis was performed using Monocle (v2.26.0) (Trapnell *et al*., 2014). Cell-cell communication networks were analyzed with CellChat (v2.1.2) (Jin *et al*., 2021) to infer intercellular signaling interactions. The SCP package (v0.5.6) facilitated visualization of cell states and interactions. All single-cell analysis steps were performed according to standard protocols as described in the original dataset publications and related method references.

Protein expression analysis

The Human Protein Atlas provided immunohistochemistry images of key lactate metabolism proteins in normal liver tissue and HCC samples (Uhlén *et al.,* 2015).

Tissue microarray immunohistochemistry

A tissue microarray of 50 HCC and matched normal samples was stained by IHC for LDHA and HDAC2 (Maixin, China). Tissue samples were collected from patients who underwent surgical resection of HCC. All patients were pathologically diagnosed with HCC. Patients with complete clinicopathological data and available follow-up information were included, whereas those who had received preoperative anticancer therapy or had incomplete clinical data were excluded. Adjacent normal tissues were obtained from non-tumorous liver tissues and were pathologically confirmed to be free of tumor involvement. Staining intensity and the percentage of positive cells were assessed to calculate the staining index (SI), categorizing samples into low ($SI \leq 4$) or high ($SI \geq 6$) expression groups.

Survival analysis

Kaplan-Meier plots were used to analyze survival differences using the log-rank test (Kaplan-Meier Plotter). The survival and survminer R packages enabled other survival analyses. Alluvial plots were generated by ggalluvial (Brunson, 2020).

Correlation analysis

ggstatsplot visualized gene correlation maps. Pheatmap displayed multi-gene correlations. ggstatsplot plotted gene expression versus immune score correlations. Spearman correlation analysis was used for non-normal quantitative data. $P < 0.05$ indicated significance.

Nomogram development

Variables for nomogram construction were identified by univariate and multivariate Cox regression. Forest plots displayed the HR and 95% CI (forestplot package). A nomogram predicting survival was built by multivariate Cox regression (rms package).

Statistical analysis

SPSS 22.0 was used to perform statistical analysis. Data are expressed as mean ± SD. Group comparisons were performed using Student's t-tests, the Wilcoxon test, one-way ANOVA, or the Kruskal-Wallis tests, while categorical variables were analyzed with Chi-square tests. A p-value < 0.05 was considered statistically significant.

RESULTS

A core enzyme of lactate metabolism influences gene expression profile and composition of the TIME in HCC

We investigated whether the core lactate metabolism enzyme LDHA influences the gene expression profile in HCC. The HCC cohort was stratified into LDHA high- and low-expression groups, which revealed distinct sets of differentially expressed genes (Fig. 1A, 1B). Notably, SPP1, CRP, SPINK1, CXCL1 and CA9 were significantly upregulated in the high-expression group, whereas SPP2, CYP7A1 and TTR were upregulated in the low-expression group. Gene Ontology (GO) and Kyoto Encyclopedia of Genes and Genomes (KEGG) enrichment analyses indicated significant activation of pathways related to cytokine–cytokine receptor interaction, response to hypoxia and decreased oxygen levels in the LDHA high-expression group (Fig. 1C). LDHA expression levels also affected key biological processes, including cellular response to hypoxia, tumor proliferation and ferroptosis (Fig. S1).

Based on these findings, we further examined changes in the HCC tumor immune microenvironment (TIME). Analysis of the TIME revealed significant differences between the two LDHA groups, particularly in the composition of immune cell populations (Fig. 1D, 1E), suggesting that LDHA expression substantially impacts the TIME. Correlation analysis demonstrated a significant relationship between LDHA levels and key TIME components in HCC (Fig. 1F). Moreover, LDHA expression was associated with differential expression of immune checkpoint genes between the high- and low-expression groups (Fig. 1G).

LDHA expression levels affect HCC cell proliferation, migration and invasion in vitro

Subsequently, we evaluated the effects of LDHA expression on HCC cell functions in vitro. CCK-8 assays demonstrated that LDHA knockdown significantly reduced the proliferation of HepG2 and Huh7 cells (Fig. 2A), whereas LDHA overexpression markedly increased their proliferative capacity (Fig. 2B). Consistently, EdU incorporation assays showed that LDHA knockdown

significantly decreased proliferative activity in both cell lines (Fig. 2C), while LDHA overexpression enhanced it (Fig. 2D).

Wound healing assays further revealed that silencing LDHA expression markedly suppressed the migratory ability of HepG2 and Huh7 cells (Fig. 3A), whereas LDHA overexpression promoted cell migration (Fig. 3B). Similarly, Transwell invasion assays indicated that LDHA knockdown significantly impaired the invasive potential of both cell lines (Fig. 3C), whereas LDHA overexpression enhanced their invasion capacity (Fig. 3D).

Key lactate metabolism drivers are clinically correlated with clinical features of HCC

To further clarify the relationship between lactate metabolism and HCC progression, we analyzed whether expression of the core lactate metabolism enzyme LDHA was associated with clinicopathological variables in HCC patients (Fig. 4A and Table 1). LDHA expression showed a significant correlation with patient survival status ($p = 0.042$), while age and TNM stage did not, suggesting that LDHA may independently influence HCC prognosis. However, LDHA expression was significantly associated with tumor stage ($p < 0.005$) (Fig. 4B), highlighting its potential role in HCC development. Kaplan–Meier survival analysis further demonstrated that patients with higher LDHA expression had significantly poorer overall survival ($p < 0.001$) (Fig. 4C).

Next, we investigated whether the broader lactate metabolic process (LMP) was implicated in HCC progression. A gene set comprising lactate metabolism-related genes (e.g., ACTN3, GATD1, HAGH, HIF1A, LDHA, LDHAL6B, LDHB, LDHC, LDHD, PARK7, PER2, PFKFB2, PNKD, SLC25A12, TIGAR and TP53) was analyzed. Survival analysis revealed that the expression levels of most LMP genes, excluding LDHAL6B, LDHC and PARK7, were significantly correlated with poorer prognosis and shorter overall survival (OS). In contrast, higher expression of HAGH, LDHD and TP53 was associated with better prognosis (Fig. 4D). Immunohistochemistry further confirmed diverse expression profiles of these genes in HCC tissues compared to normal liver samples (Fig. 4E).

LMPA is associated with poor prognosis and TIME remodeling in HCC patients

Based on the above findings, we hypothesized that overall lactate metabolic process activity (LMPA) may influence HCC progression. To test this, we first evaluated the correlations among lactate metabolism-related genes (Fig. 5A). Notably, LDHA showed a strong positive correlation with HIF1A ($r = 0.53$), suggesting a link between hypoxia and lactate metabolism in HCC. TIGAR was also positively correlated with HIF1A ($r = 0.55$), whereas TP53 was negatively correlated with HAGH ($r = –0.38$), indicating potential internal regulatory relationships within the lactate metabolic process.

Considering the potential impact of LMPA on TIME remodeling and patient prognosis, we constructed an LMPA prognostic model (Fig. 5B). The model's Akaike information criterion (AIC) was 1302.97. Patients in the high-risk group had significantly shorter overall survival than those in the low-risk group ($p < 0.001$) (Fig. 5C), indicating poorer prognosis. The ROC curve and AUC values demonstrated that the LMPA model had strong predictive performance and accuracy (Fig. 5D). Analysis of key TIME components showed that B cells, CD4+ T cells, neutrophils, macrophages and myeloid dendritic cells were significantly correlated with the LMPA-based risk score (Fig. 5E). Additionally, a nomogram incorporating univariate and multivariate Cox regression analyses was developed to predict 1-, 3- and 5-year overall survival, with calibration curves indicating good predictive performance (Figs. 5F–H).

LMPA-based molecular subtypes of HCC are associated with global protein lactylation

Next, we investigated whether HCC molecular subtypes based on LMPA could influence global protein lactylation. Consensus clustering analysis demonstrated good stability at $k = 3$, identifying three distinct subtypes: C1, C2 and C3 (Fig. 6A–B). Principal component analysis and heatmap visualization confirmed clear separation among these clusters (Fig. 6C–D). The subtypes were significantly associated with various clinicopathological features, including gender, grade and T stage (Fig. 6E). Survival analysis revealed significant differences in overall survival among the subtypes ($p = 0.0089$), with C1 exhibiting the best prognosis and C2 the worst (Fig. 6F).

Further exploration of the relationship between LMPA-based subtypes and global protein lactylation revealed that these subtypes significantly affected the expression of miR-210, a key regulator of lactate metabolism (Fig. 6G). Importantly, the subtypes also influenced the expression of HDACs, SIRTs and p300 (Fig. 6H–J), which are critical enzymes involved in histone lactylation, underscoring the relevance of LMPA to epigenetic regulation in HCC. Consistent with earlier enrichment analyses (Fig. S1), the LMPA-based subtypes were also linked to ferroptosis pathways (Fig. 6K). Differential gene expression analysis identified subtype-specific differences in AFP, CCL20, EPCAM, HPD and SLC27A5 expression (Fig. 6L), as well as pathways related to p53 signaling, steroid metabolism and retinol metabolism (Fig. 6M).

scRNA-seq reveals diverse lactate-related metabolic reprogramming, lactylation and LMPA patterns in immune cells within the HCC TIME

We next investigated whether immune cells within the HCC TIME exhibit distinct patterns of lactate-related metabolic reprogramming, histone lactylation and LMPA. Single-cell RNA-seq analysis of the tumor core TIME revealed clear clustering of T cells, B cells, macrophages and NK cells (Fig. 7A–B).

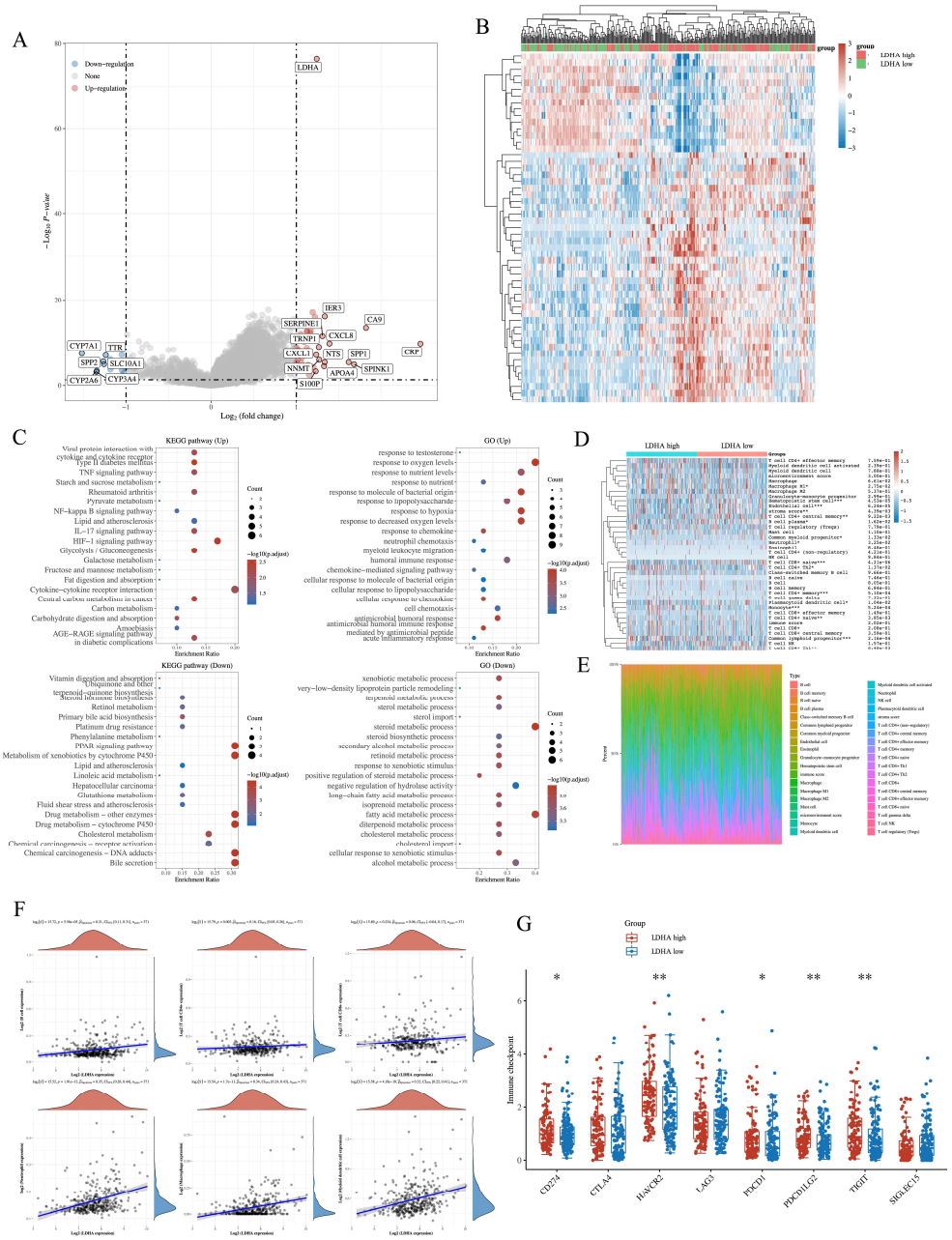

Fig. 1: A core enzyme of lactate metabolism was relevant to component of tumor immune microenvironment (TIME) in HCC. (A) The volcano plot was constructed using the fold change values and adjusted P values. Red dots indicate upregulated genes in LDHA high group; blue dots indicate downregulated genes in LDHA high group; grey dots indicate not significant; (B) The heatmap of differential gene expression, with different colors indicating the trend of gene expression across tissues. The top 50 up-regulated genes and top 50 down-regulated genes in LDHA high group were shown; (C) The enriched KEGG signaling pathways were selected to demonstrate the primary biological actions of major potential mRNA. The abscissa indicates gene ratio and the enriched pathways were presented in the ordinate. Gene ontology (GO) analysis of potential targets of mRNAs. The biological process (BP), cellular component (CC), and molecular function (MF) of potential targets were clustered based on the ClusterProfiler package in R software (version: 3.18.0). Colors represent the significance of differential enrichment and the size of the circles represents the number of genes, the larger the circle, the greater the number of genes. In the enrichment results, $p < 0.05$ or FDR < 0.05 is considered a meaningful pathway (enrichment score with −log10(P)> 1.3); (D) Immune cell score heatmap, different colors represent different expression distribution in different samples. *p < 0.05, **p < 0.01, ***p < 0.001, asterisks (*) stand for significance levels. The statistical difference between the two groups was compared through the Wilcoxon test; (E) The percentage abundance of tumor infiltrating immune cells in each sample. Different colors represent different types of immune cells. The abscissa represents the sample, and the ordinate represents the percentage of immune cell content in a single sample; (F) The correlations between gene expression and immune score were analyzed with Spearman. The abscissa represents the distribution of the gene expression or the score, and the ordinate represents the distribution of the immune score. The density curve on the right represents the trend in distribution of the immune score; the upper density curve represents the trend in distribution of the gene expression or the score. The value on the top represents the correlation p-value, correlation coefficient and correlation calculation method. (G) The heatmap of immune-checkpoint-related gene expression in LDHA high group and LDHA low group of ICGC HCC patients. The different colors represent the trend of gene expression in different samples. *p < 0.05, **p < 0.01, ***p < 0.001, asterisks (*) stand for significance levels. The statistical difference of two groups was compared through the Wilcoxon test.

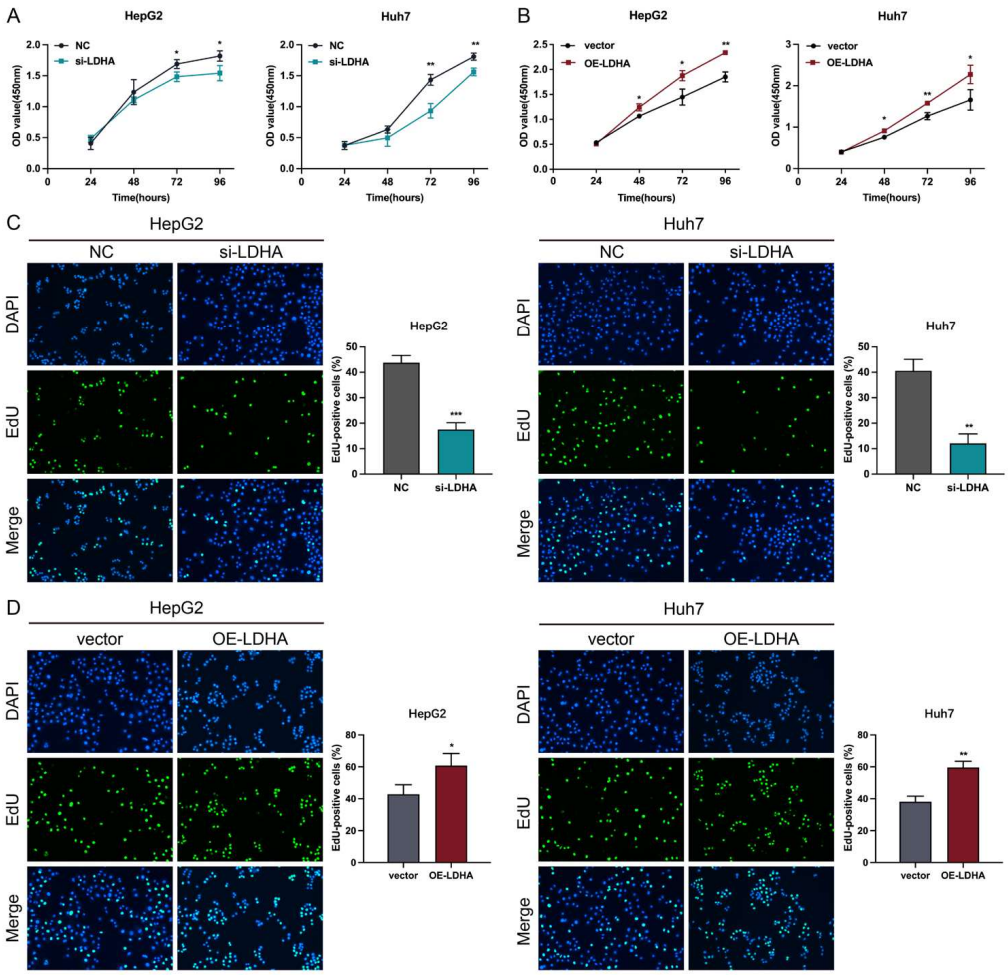

Fig. 2: Effects of LDHA expression on HCC cell proliferation.
(A) CCK8 assays of knockdown of LDHA in HCC cell lines HepG2 and Huh7; (B) CCK8 assays of overexpression of LDHA in HCC cell lines HepG2 and Huh7; (C) EdU assays of knockdown of LDHA in HCC cell lines HepG2 and Huh7; (D) EdU assays of overexpression of LDHA in HCC cell lines HepG2 and Huh7. * $p<0.05$, ** $p<0.01$.

Table 1: Relationship between LDHA expression level and clinicopathological variables in HCC patients.

	LDHA low (n=185)	LDHA high(n=186)	p-value
Alive	130	111	0.042
Dead	55	75	
Mean age, year (SD)	59.9 (12.6)	59 (14.4)	0.514
Female	54	67	0.196
Male	131	119	
T1	98	83	0.237
T2	48	47	
T3	35	45	
T4	3	10	
TX	1	1	
N0	121	131	0.323
N1	1	3	
NX	62	52	
M0	130	136	0.445
M1	1	3	
MX	54	47	

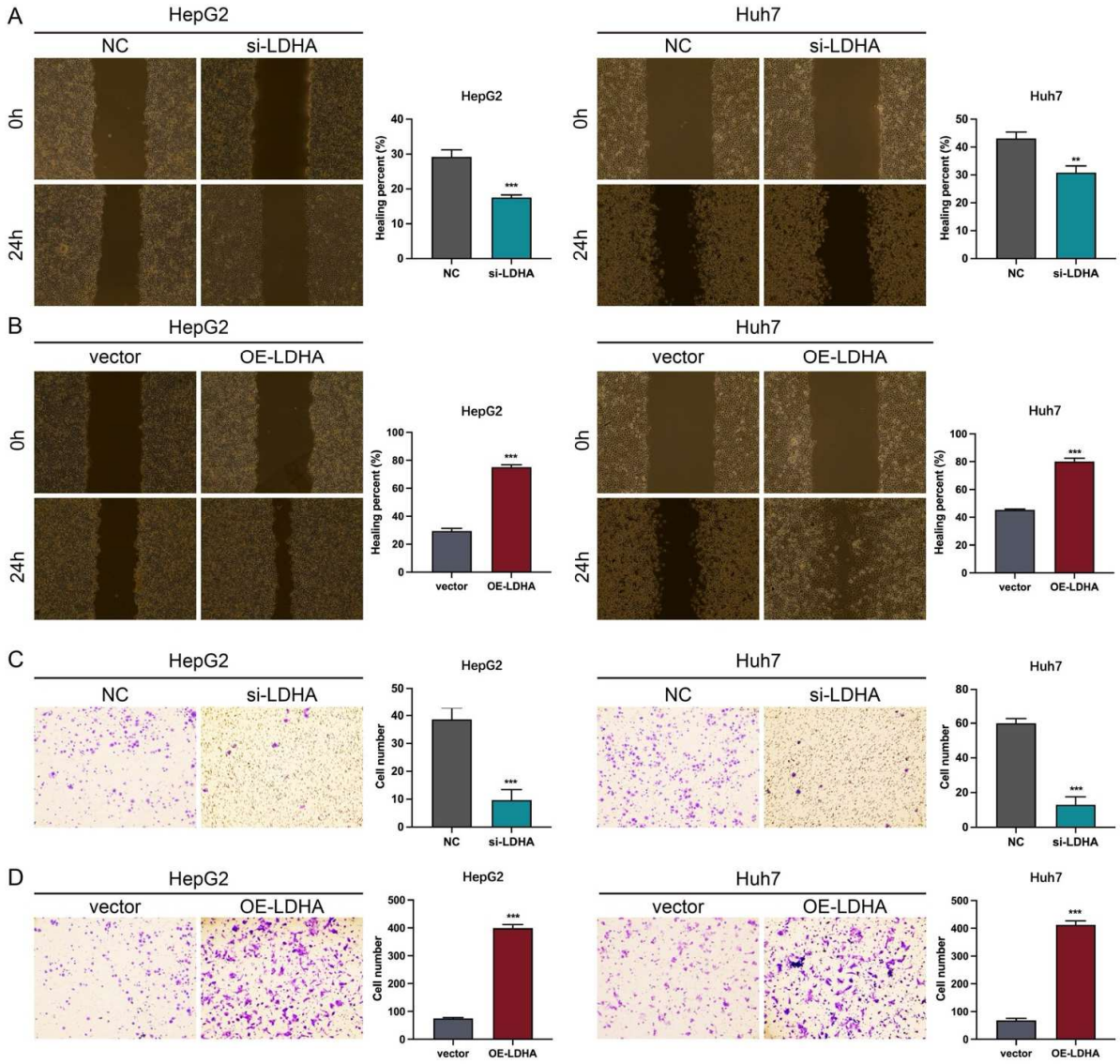

Fig. 3: Effects of LDHA expression on HCC cell migration and invasion.
(A) Wound healing assays of knockdown of LDHA in HCC cell lines HepG2 and Huh7. (B) Wound healing assays of overexpression of LDHA in HCC cell lines HepG2 and Huh7. (C) Transwell assays of knockdown of LDHA in HCC cell lines HepG2 and Huh7. (D) Transwell assays of overexpression of LDHA in HCC cell lines HepG2 and Huh7. * $p<0.05$, ** $p<0.01$.

Table 2: Cox univariable and multivariable analysis of clinicopathological variables with LDHA and HDAC2 expression in relation to OS in HCC patients.

Clinical factor	Univariable analysis			Multivariable analysis		
	HR	95%CI	p-value			
Gender (male vs. female)	1.042	0.872-1.274	0.127			
Age (>=60 vs. <60 years)	0.973	0.683-1.171	0.218			
Tumor size (vs. 0-5 cm)						
< 10, > 5 cm	1.436	0.783-1.983	0.081			
> 10 cm	1.921	1.394-2.204	0.056			
Vascular invasion (Positive vs. Negative)	1.084	0.753-1.393	0.108			
Metastasis (Positive vs. Negative)	2.284	1.693-4.385	< 0.001	2.432	1.218-4.233	< 0.001
Stage (III-IV vs. I-II)	1.520	0.922-2.013	0.064			
LDHA expression (High vs. Low)	3.084	2.094-5.274	< 0.001	3.201	2.132-5.341	< 0.001
HDAC2 expression (High vs. Low)	2.809	1.342-3.427	< 0.001	2.941	1.532-3.353	< 0.001

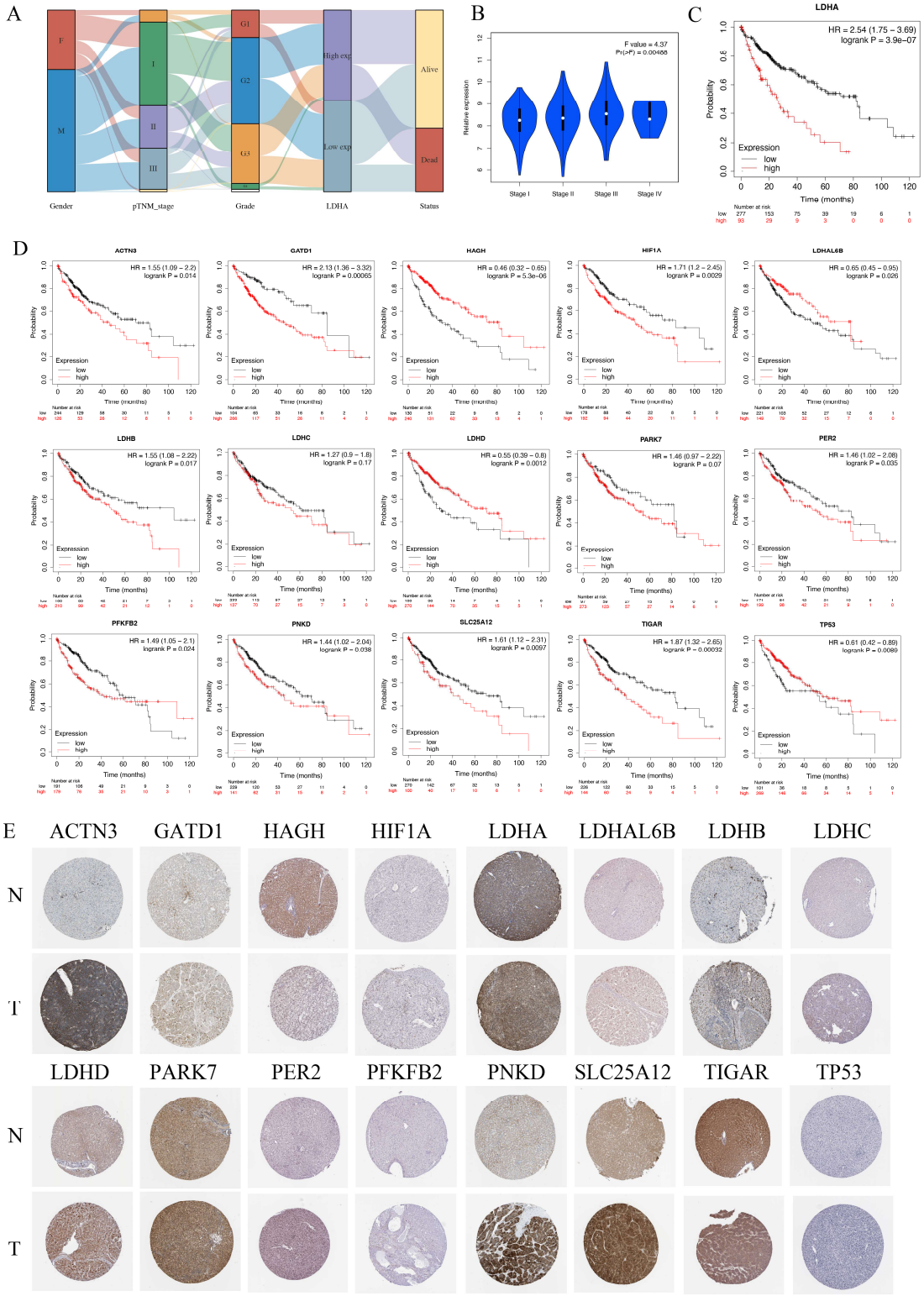

Fig. 4: Key drivers of the lactate metabolic process are clinically associated with HCC.
(A) Sankey plot of the relationship between LDHA expression and clinical features of HCC. Each row represented a feature variable, a different color represented a different type or stage and lines represented the distribution of the same sample in different feature variables; (B) Violin plot of relationship of LDHA expression and HCC clinical stage; (C) Kaplan-Meier survival analysis of the different groups of HCC patients, comparison among different groups was made by log-rank test. HR (95%Cl) for high and low relative LDHA gene expression groups; (D) Kaplan-Meier survival analysis of the different groups of HCC patients, comparison among different groups was made by log-rank test. HR (95%Cl) for high and low relative gene expression groups; (E) Immunohistochemistry (IHC) of given gene expression in normal liver (N) sample and HCC tissue (T).

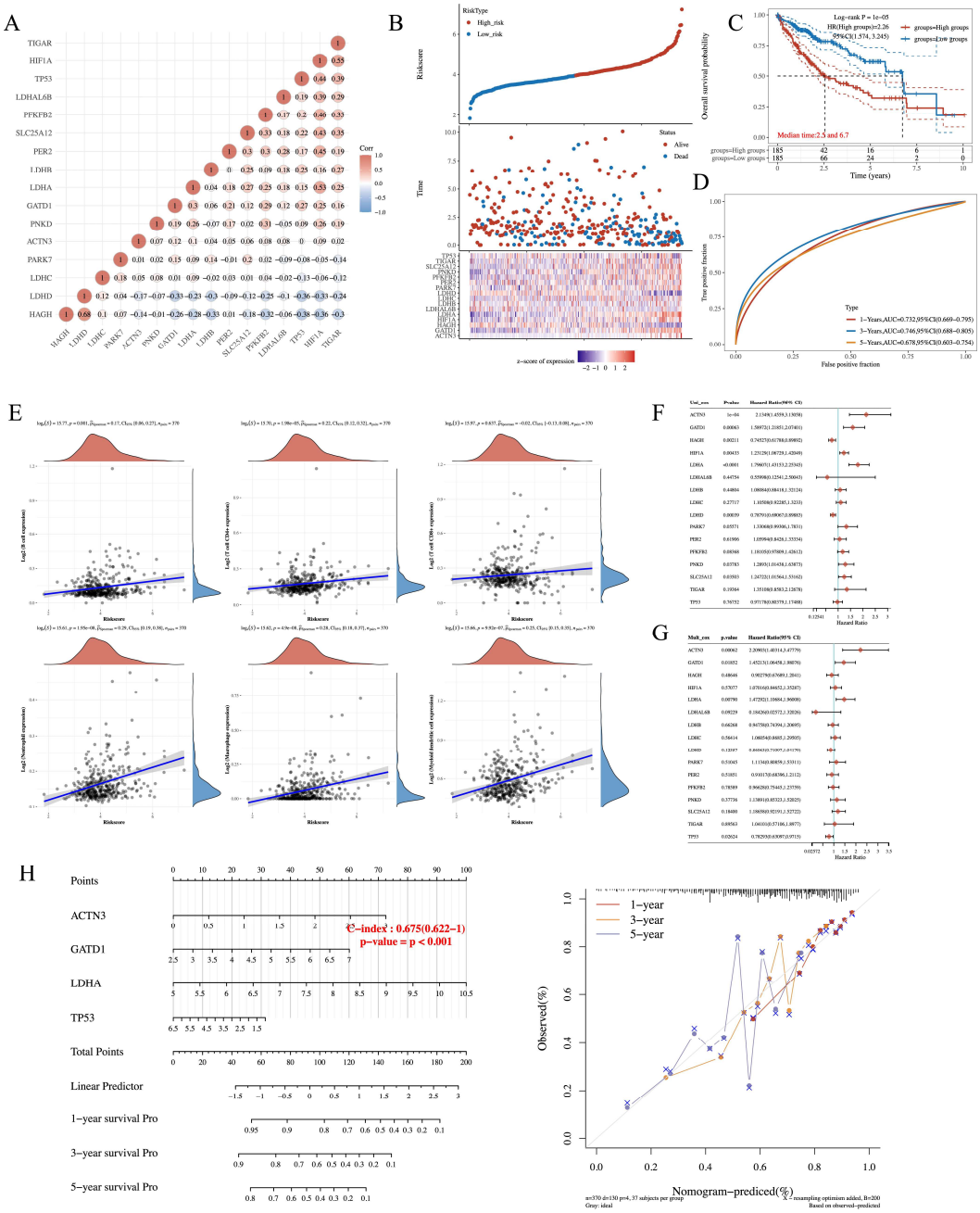

Fig. 5: LMPA is associated with poor prognosis and TIME remodeling in HCC patients.
(A) The correlations among lactate metabolic process genes in HCC are exhibited by a heatmap. The abscissa and ordinate represent genes, different colors represent different correlation coefficients (blue represents positive correlation, whereas red represents negative correlation) and the darker the color, the stronger the relation; (B) The risk score, survival time and survival status of LMPA model in HCC. The top scatterplot represents the risk score from low to high. Different colors represent different groups. The scatter plot distribution represents the risk score of different HCC patients corresponding to the survival time and survival status. The bottom heatmap is the gene expression from the LMPA model; (C) Kaplan-Meier survival analysis of the LMPA model of HCC patients, comparison among different groups was made by log-rank test. HR (High exp) represents the hazard ratio of the low-expression sample relatives to the high-expression sample. HR> 1 indicates the gene is a risk factor, and HR<1 indicates the gene is a protective factor. HR (95%CI), the median survival time (LT50) for different groups, in years. (D) The ROC curve and AUC of the LMPA model. Higher AUC values correspond to greater predictive power; (E) The correlations between LMPA risk score and immune score were analyzed with Spearman. The abscissa represents the distribution of the gene expression or the score, and the ordinate represents the distribution of the immune score. The density curve on the right represents the trend in distribution of the immune score; the upper density curve represents the trend in distribution of the gene expression or the score. The value on the top represents the correlation *p-value*, correlation coefficient and correlation calculation method; (F) The *p-value*, HR and confidence interval were analyzed by univariate Cox regression; (G) The *p-value*, HR and confidence interval analyzed by multivariate Cox regression; (H) Nomogram predicting the 1-year，3-year and 5-year overall survival of HCC patients; (I) Calibration curve for the overall survival nomogram model. The dashed diagonal line represents the ideal nomogram, and the blue line, red line and orange line represent the 1-year，3-year and 5-year of the observed nomogram.

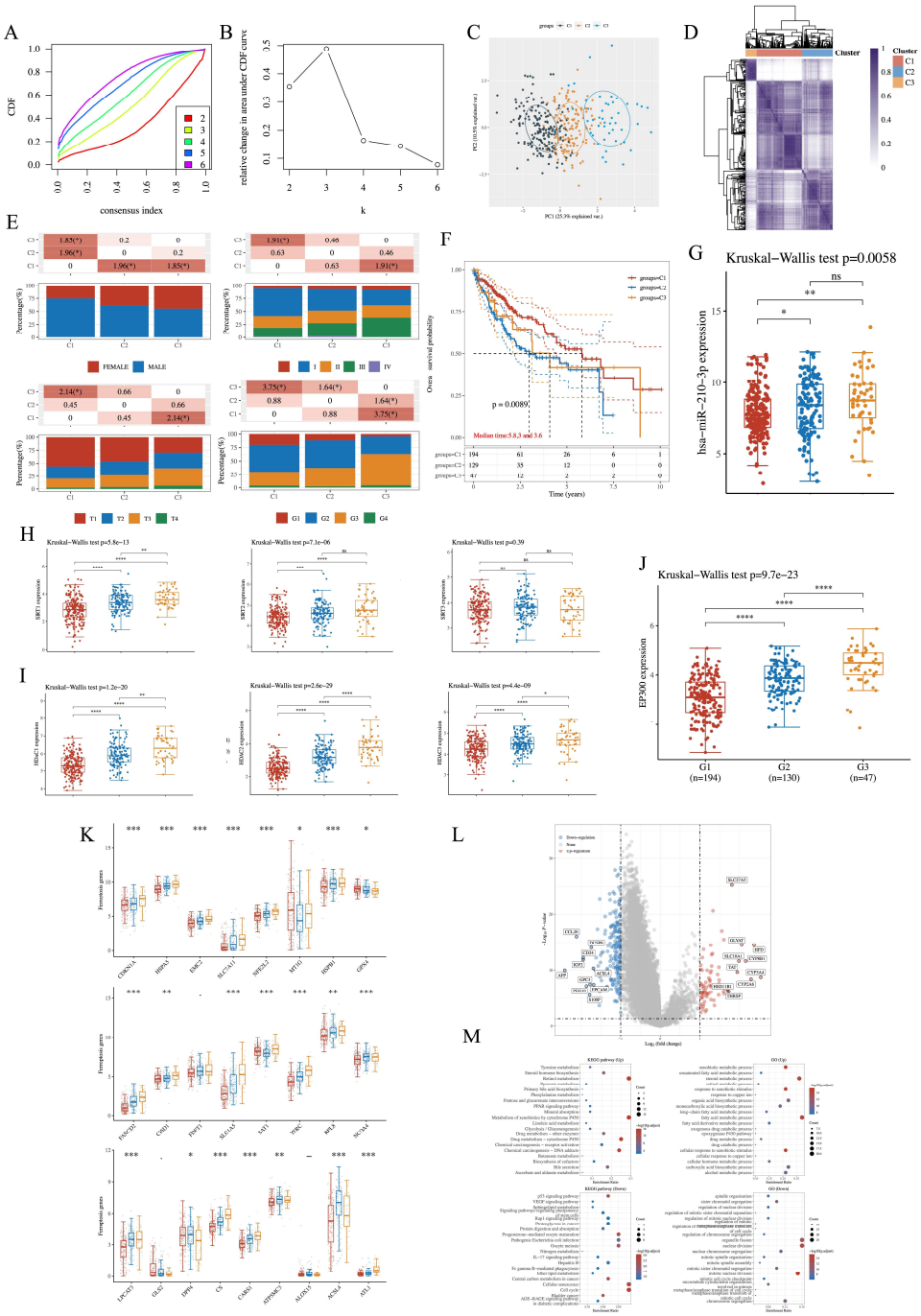

Fig. 6: LMPA-based molecular subtypes of HCC are associated with global protein lactylation.
(A) Consensus clustering cumulative distribution function (CDF) of molecular subtypes of HCC patients. (B) relative change in the area under the CDF curve (CDF Delta area). The relative change in area under the cumulative distribution function (CDF) curves when cluster number varying from k-1 to k. The abscissa represents category number k, and the ordinate represents the relative change in the area. (C) Principal component analysis (PCA) of HCC patients in subgroups. (D) Consistency of clustering results heatmap (k = 3), Rows and columns represent samples, the different colors represent different types. And the expression heatmap of genes in different subgroups, red represents high expression, and blue represents low expression. (E) The distribution of clinical characteristics in the samples from different groups. The abscissa represents samples from different groups, and the ordinate represents the percentage of clinical sample information in corresponding group, different colors represent different clinical information. The above table represents the distribution of a clinical feature between arbitrary two groups, and the significance *p-value* was analyzed by chi-square test, where the value is displayed as -log10 (*p-value*). Marked with * indicated a significant difference in the distribution of the clinical features between the two groups ($p < 0.05$). (F) Survival analysis of C1, C2 and C3 groups. (G) The expression distribution of miR-210-3p in different groups. (H) The expression distribution of SIRTs family in different groups. (I) The expression distribution of HDACs family in different groups. (J) The expression distribution of p300 in different groups. (K) The expression distribution of ferroptosis family in different groups. (L) The volcano plot was constructed using the fold change values and P-adjust. Red dots indicate upregulated genes in C1 group; blue dots indicate downregulated genes in C2 group; grey dots indicate not significant. (M) GO and KEGG enrichment analyses of differentially expressed genes between the C1 and C2 groups.

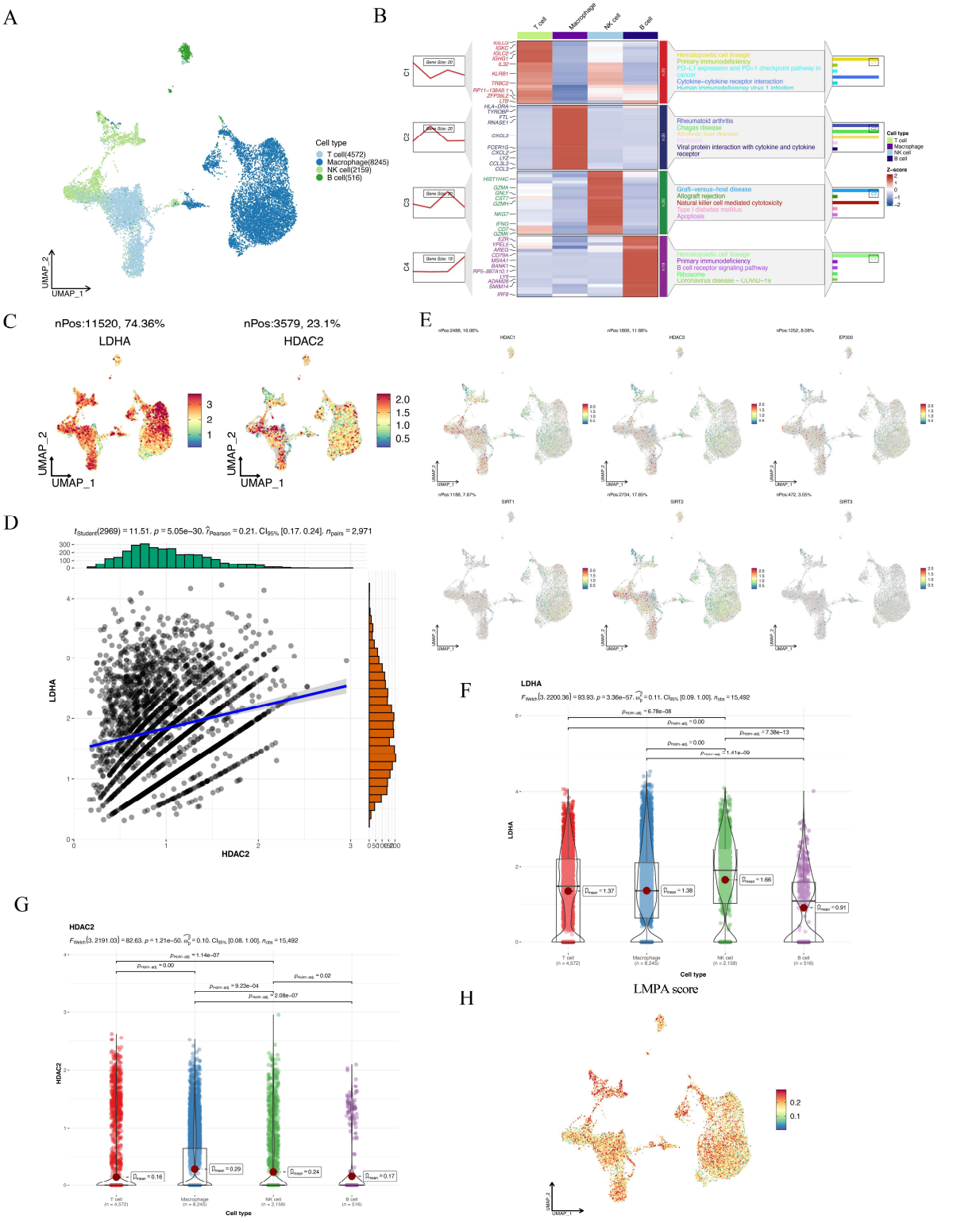

Fig. 7: Single-cell RNA-seq (scRNA-seq) revealed diverse lactate related metabolic reprogramming, lactylation modification and LMPA patterns of immune cells in TIME of HCC.

(A) UMAP of scRNA-seq of HCC core tumor TIME in GSE140228; (B) Heatmap plot of different expressed genes and enrichment pathways in each cell type; (C) LDHA and HDAC2 expression in HCC TIME shown on the UMAP; (D) Correlation between LDHA and HDAC2 expression in single cells; (E) Lactylation modification related gene expression in each cell type is shown in the UMAP; (F) Violin plot of LDHA expression in each cell type; (G) Violin plot of LDHA expression in each cell type; (H) LMPA score in HCC TIME showing in the UMAP.

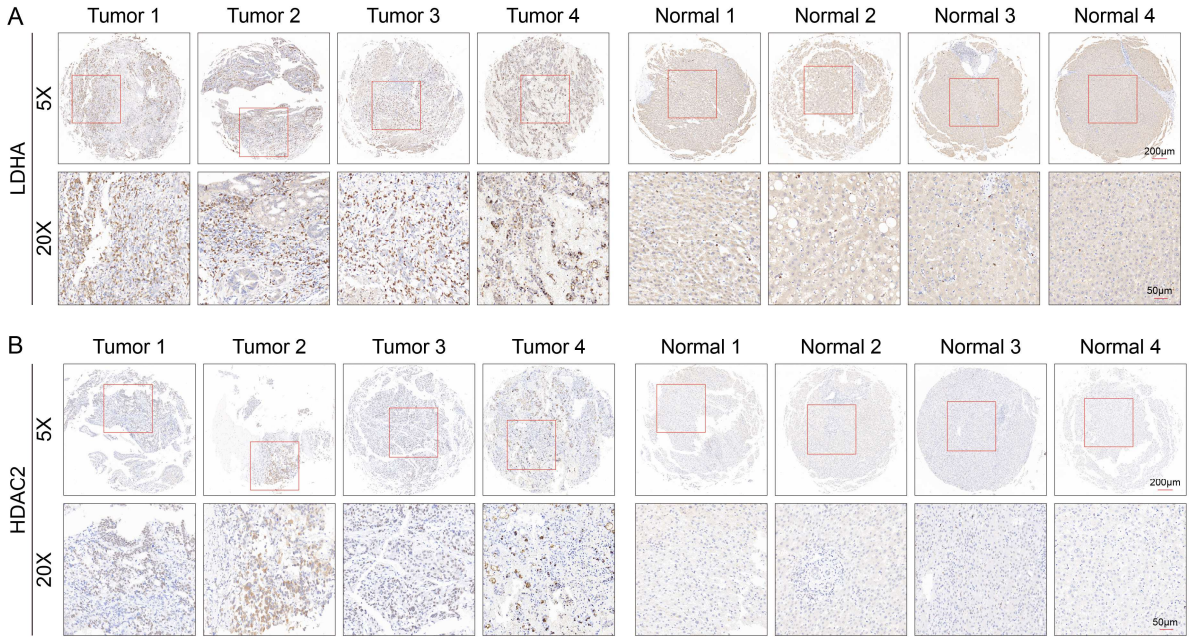

Fig. 8: IHC of (A) LDHA and (B) HDAC2 protein staining in tissue microarray in HCC tissue and matched adjacent normal tissue.

Each immune cell type displayed unique LDHA and HDAC2 expression profiles (Fig. 7C). Notably, LDHA and HDAC2 expression levels were significantly correlated (Fig. 7D), whereas other lactylation-related genes showed relatively low expression (Fig. 7E), suggesting that HDAC2 may play a key role in regulating lactylation within the TIME. Among the immune cell types, NK cells exhibited the highest LDHA expression (Fig. 7F), while macrophages showed the highest HDAC2 levels (Fig. 7G). Additionally, each immune cell subset demonstrated distinct LMPA patterns in the HCC TIME (Fig. 7H).

LDHA and HDAC2 expression are clinically correlated in HCC patients

We further examined the correlation between LDHA and HDAC2 expression and HCC patient clinicopathological characteristics using immunohistochemistry on tissue microarrays (Fig. 8). Univariate analysis showed that LDHA expression ($p < 0.001$), HDAC2 expression ($p < 0.001$) and metastasis ($p < 0.001$) were significantly associated with overall survival (OS) in HCC patients (Table 2). Subsequent multivariate analysis confirmed that LDHA expression, HDAC2 expression and metastasis remained independent risk factors for OS (all $p < 0.001$).

scRNA-seq reveals diverse protein lactylation and LMPA patterns in lymphoid T cell subtypes during HCC progression

Finally, we explored whether global protein lactylation and LMPA patterns differ across lymphoid T cell subtypes during HCC progression. Dimensionality reduction analysis of the HCC TIME revealed a complex composition of T cell subsets (Fig. 9A). Cell–cell communication analysis demonstrated intricate interactions among the T cell subtypes, primarily mediated by CCL and PARs signaling pathways (Fig. 9B–E). Pseudotime trajectory analysis further showed continuous evolutionary trajectories for each subtype, accompanied by distinct global protein lactylation and LMPA patterns (Fig. 9F–H).

DISCUSSION

HCC is among the most prevalent and fatal malignancies worldwide, characterized by rapid disease progression, high recurrence rates and poor prognosis for most patients (Sartoris *et al*., 2021; Yeh *et al*., 2021). Despite significant advances in surgical resection, locoregional therapies, and systemic treatments, including the multi-kinase inhibitor sorafenib and anti-PD-1-based combination immunotherapy (Huang *et al*., 2020; Xu *et al*., 2018), overall survival benefits remain modest and many patients still have limited treatment options once resistance develops. These limitations highlight an urgent need for innovative therapeutic strategies that go beyond conventional approaches and tackle the underlying biological processes driving tumor progression and immune evasion (Yeo *et al*., 2025; Zheng *et al*., 2025). In this context, our study identifies lactate metabolism as a critical and potentially actionable metabolic pathway that may be exploited to develop more effective and personalized treatments for HCC. By focusing on the role of lactate as both a metabolic byproduct and a key regulator of the tumor microenvironment, our findings provide new insights into how targeting lactate-related metabolic reprogramming could complement existing therapies and improve patient outcomes.

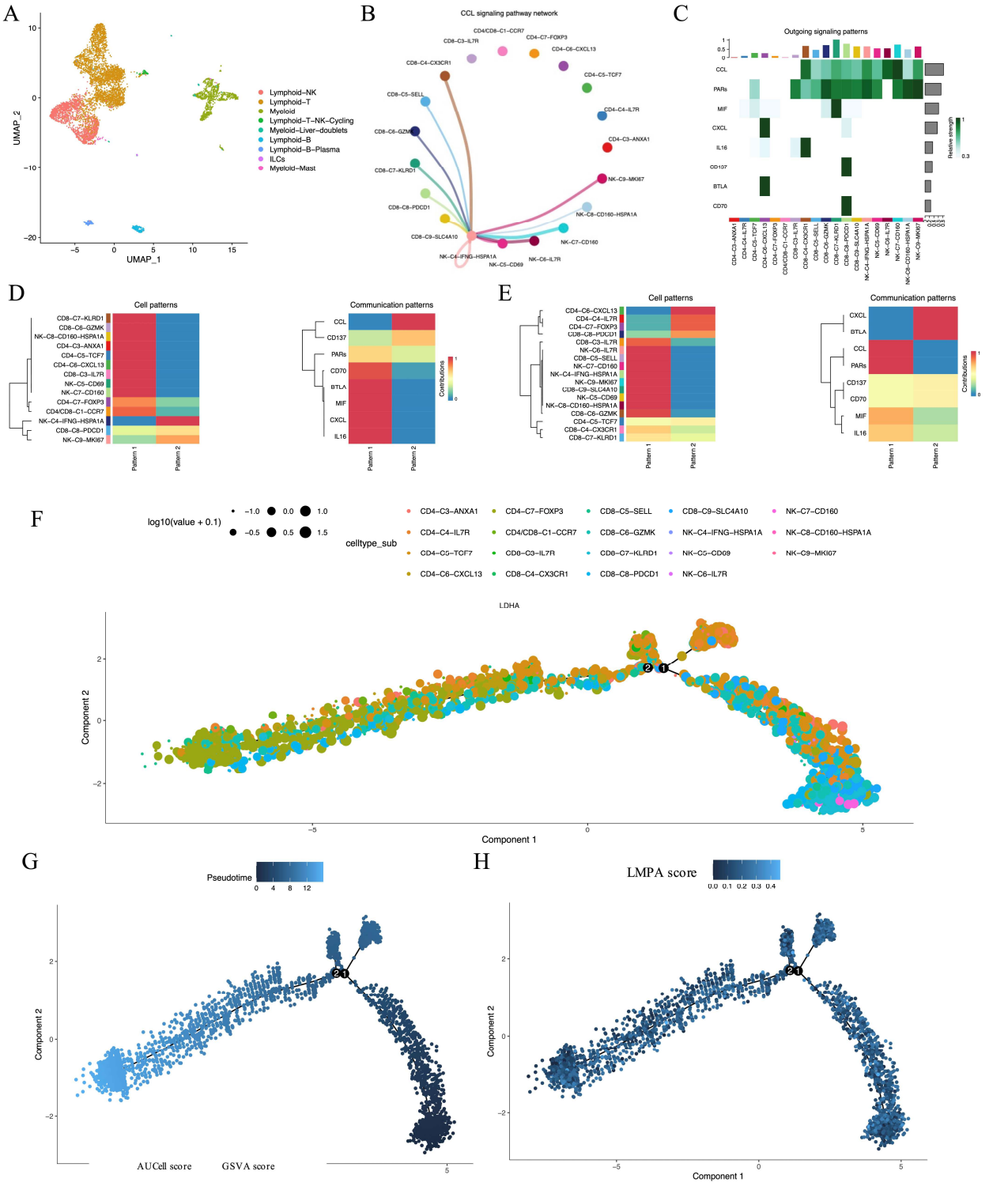

Fig. 9: scRNA-seq revealed diverse protein lactylation and LMPA patterns of lymphoid T cell during progression of HCC.

(A) UMAP of scRNA-seq of HCC TIME in GSE149614. (B) CCL signaling pathway network analysis of lymphoid T cell in HCC TIME. (C) Outgoing pattern analysis of lymphoid T cell. (D) Cell patterns and incoming communication patterns of lymphoid T cell. (E) Cell patterns and outgoing communication patterns of lymphoid T cell. (F) Pseudotime analysis of lymphoid T cell by cell subtypes (color) and LDHA expression (size of points). (G) Pseudotime analysis of lymphoid T cell by pseudotime. (H) Pseudotime analysis of lymphoid T cell by LMPA score.

Lactate, traditionally regarded as the end product of anaerobic glycolysis, is now recognized as a circulating energy source and signaling molecule within the tumor microenvironment (Cui *et al*., 2025; Rabinowitz and Enerback, 2020). In the context of tumorigenesis and metastasis, accumulating evidence suggests that aberrant lactate production and accumulation can profoundly influence cancer cell behavior and intercellular communication (Bergers and Fendt, 2021). Metabolic reprogramming, including enhanced lactate metabolism, is particularly prevalent during HCC initiation and progression, providing multiple metabolic nodes that could serve as promising therapeutic entry points (Du *et al*., 2022).

Recent evidence suggests that excessive lactate accumulation in the tumor microenvironment can serve as a substrate for histone lactylation, a novel epigenetic modification mediated by the lactyltransferase activity of p300 (Ziogas *et al*., 2025). In our study, we demonstrate that variations in LMPA are closely linked to differences in gene expression profiles, survival outcomes and the immune contexture of HCC patients. This underscores the notion that lactate metabolism is not merely a bystander but an active contributor to tumor growth and immune evasion. A deeper understanding of the specific mechanisms by which lactate metabolism shapes HCC biology may ultimately guide the development of novel treatment strategies that disrupt these metabolic-immune interactions and improve patient prognosis. Prognostic models are important tools for predicting survival in patients with HCC. A TP53-associated immune model identified low/high risk subgroups (Long *et al*., 2019). Ferroptosis and iron metabolism signatures predicted HCC prognosis and the TIME (Tang *et al*., 2020). A CTNNB1-associated model efficiently predicted survival (Huo *et al*., 2021). We found differential LMPA significantly associated with patient survival time. Our LMPA-based model showed a strong correlation with survival, potentially enabling earlier intervention.

Metabolic reprogramming provides the energy for the progression of HCC (Liu *et al*., 2024). Comparative analyses between HCC patients with low and high LMPA revealed substantial differences in the composition and distribution of key immune cell populations within the TIME, including B cells, CD4+ T cells, neutrophils, macrophages and dendritic cells. These shifts suggest that heightened lactate metabolism may actively shape an immunosuppressive or dysfunctional TIME by modulating the recruitment, activation, or suppression of specific immune cell subsets. Furthermore, our single-cell RNA sequencing results provide additional resolution by demonstrating that distinct LMPA patterns exist across different immune cell types, highlighting the heterogeneity of metabolic reprogramming at the single-cell level. Together, these findings support the notion that lactate-related metabolic reprogramming directly contributes to TIME remodeling in HCC, which is consistent with prior evidence indicating that dysregulated immunometabolism and elevated lactate are central drivers of immune evasion and tumor progression (Ding *et al*., 2025; Giannone *et al*., 2020). Prior work has shown that PIWIL1 governs the interplay between cancer cell fatty acid metabolism and the immunosuppressive microenvironment in HCC (Wang *et al*., 2021), whereas our study extends this concept by demonstrating how lactate-related metabolic reprogramming and histone lactylation similarly reshape immune cell function and TIME composition. A better understanding of these lactate-driven metabolic-immune interactions, especially the role of histone lactylation in regulating immune cell phenotypes, may guide the rational development of novel TIME-targeting immunotherapies. Importantly, our findings suggest that combining metabolic interventions, such as LDHA inhibition, with immune checkpoint blockade could be a promising approach for HCC treatment. However, further preclinical studies and clinical trials will be needed to evaluate the safety, feasibility and potential challenges of translating this strategy into effective therapies.

Distinct molecular subtypes have important implications for the treatment of HCC (Cappuyns *et al*., 2025; Chen *et al*., 2024). Our identification of distinct HCC molecular subtypes based on LMPA further underscores the biological significance of lactate-related metabolic reprogramming. These subtypes were strongly associated with differential global protein lactylation, suggesting that elevated LMPA may promote epigenetic modifications that impact gene expression not only in tumor cells but also in various immune cell populations within the TIME. This link suggests that aberrant lactylation may serve as an additional layer of immunometabolic regulation that contributes to immune cell dysfunction and tumor immune escape. Therefore, therapeutically targeting LMPA holds promise not only for disrupting metabolic pathways fueling tumor growth but also for reducing pathological lactylation within the TIME, potentially restoring a more favorable immune landscape. This dual effect highlights the potential of LMPA modulation as a novel strategy to complement current immunotherapies and enhance their efficacy in patients with HCC.

Limitations of this study include the absence of *in-vivo* experiments, which restricts the physiological validation of our findings. Although our multi-omics analyses provide important preliminary evidence, further animal studies, such as murine HCC models or patient-derived xenografts, are necessary to confirm the causal impact of lactate metabolism and lactylation on tumor progression and immune remodeling. Additionally, although our study shows a potential association between LMPA and lactylation, the precise mechanisms by which this epigenetic modification regulates immune cell gene expression and function within the TIME remain to be

elucidated through functional assays. We also acknowledge the potential biases inherent in public bulk and single-cell datasets, including sample heterogeneity, batch effects and limited patient diversity, which may affect generalizability. Moreover, while our single-cell analysis provides valuable insight into cell-specific metabolic patterns, further studies are needed to functionally validate immune cell phenotypes, particularly using direct *in-situ* or *ex-vivo* experiments. Future work addressing these limitations will help to translate our findings into clinically meaningful applications.

CONCLUSION

In summary, our study reveals that lactate-related metabolic reprogramming actively increases global protein lactylation and reshapes the TIME in HCC, thereby potentially promoting immune evasion and tumor progression. By integrating bulk and single-cell transcriptomic analyses with in vitro functional validation, we identify LDHA and LMPA as promising biomarkers and therapeutic targets. These findings provide new insights into the epigenetic and immunometabolic crosstalk in HCC. Future research should focus on functional validation of specific lactylation targets in immune cells, in vivo testing of LDHA inhibition strategies and evaluation of combination therapies that target lactate metabolism alongside immune checkpoint blockade. Such efforts may help translate these mechanistic insights into more effective immunotherapeutic approaches for HCC patients.

Acknowledgments
All authors acknowledge the contributions from the TCGA and GEO projects.

Authors' contributions
Taiyu Xia and Ya Li: Methodology, software, formal analysis, investigation and writing original draft preparation. Zhengwei Song and Xuemei Zhao: Substantial contributions to the conception of the work and substantially revised it. All authors reviewed the manuscript.

Funding
There was no funding.

Data availability statement
All data generated or analyzed during the present study are included in this published article or are available from the corresponding author on reasonable request.

Ethical approval
The studies involving human participants were reviewed and approved by the Ethics Committee of the People's Hospital of Dazu (Approval No. 2300076645).

Conflict of interest
None to declare

Supplementary data
https://www.pjps.pk/uploads/2026/05/SUP1777635488.pdf

REFERENCES

Aran D, Hu Z and Butte AJ (2017). xCell: Digitally portraying the tissue cellular heterogeneity landscape. *Genome Biol.*, **18**(1): 220.

Bergers G and Fendt SM (2021). The metabolism of cancer cells during metastasis. *Nat. Rev. Cancer*, **21**(3): 162-180.

Blanche P, Dartigues JF and Jacqmin-Gadda H (2013). Estimating and comparing time-dependent areas under receiver operating characteristic curves for censored event times with competing risks. *Stat. Med.*, **32**(30): 5381-5397.

Brunson JC (2020). ggalluvial: Layered grammar for alluvial plots. J. *Open Source Softw.*, **5**(49): 2017.

Cai K, Fang Y, Zhang Y, Liu J, Ye Q, Ding L and Cai X (2024). Cetylpyridinium chloride inhibits hepatocellular carcinoma growth and metastasis through regulating epithelial-mesenchymal transition and apoptosis. *PLoS One,* **19**(9): e0310391.

Cappuyns S, Pique-Gili M, Esteban-Fabro R, Philips G, Balaseviciute U, Pinyol R, Gris-Oliver A, Vandecaveye V, Abril-Fornaguera J, Montironi C, Bassaganyas L, Peix J, Zeitlhoefler M, Mesropian A, Huguet-Pradell J, Haber PK, Figueiredo I, Ioannou G, Gonzalez-Kozlova E, D'Alessio A, Mohr R, Meyer T, Lachenmayer A, Marquardt JU, Reeves HL, Edeline J, Finkelmeier F, Trojan J, Galle PR, Foerster F, Minguez B, Montal R, Gnjatic S, Pinato DJ, Heikenwalder M, Verslype C, Van Cutsem E, Lambrechts D, Villanueva A, Dekervel J and Llovet JM (2025). Single-cell RNA sequencing-derived signatures define response patterns to atezolizumab + bevacizumab in advanced hepatocellular carcinoma. *J. Hepatol.*, **82**(6): 1036-1049.

Chen J, Huang Z, Chen Y, Tian H, Chai P, Shen Y, Yao Y, Xu S, Ge S and Jia R (2025). Lactate and lactylation in cancer. *Signal Transduct Target Ther.*, **10**(1): 38.

Chen Y, Deng X, Li Y, Han Y, Peng Y, Wu W, Wang X, Ma J, Hu E, Zhou X, Shen E, Zeng S, Cai C, Qin Y and Shen H (2024). Comprehensive molecular classification predicted microenvironment profiles and therapy response for HCC. *Hepatology,* **80**(3): 536-551.

Chen Z, Xie H, Hu M, Huang T, Hu Y, Sang N and Zhao Y (2020). Recent progress in treatment of hepatocellular carcinoma. *Am. J. Cancer Res.*, **10**(9): 2993-3036.

Cui Y, Liu J, Wang X, Wu Y, Chang Y, Hu X and Zhao W (2025). Baicalin attenuates the immune escape of oral squamous cell carcinoma by reducing lactate accumulation in tumor microenvironment. *J. Adv Res*., doi: 10.1016/j.jare.2025.01.021. In press.

Deng J, Li Y, Yin L, Liu S, Li Y, Liao W, Mu L, Luo X and Qin J (2025). Histone lactylation enhances GCLC expression and thus promotes chemoresistance of

colorectal cancer stem cells through inhibiting ferroptosis. *Cell Death Dis.*, **16**(1): 193.

Ding CH, Yan FZ, Xu BN, Qian H, Hong XL, Liu SQ, Luo YY, Wu SH, Cai LY, Zhang X and Xie WF (2025). PRMT3 drives PD-L1-mediated immune escape through activating PDHK1-regulated glycolysis in hepatocellular carcinoma. *Cell Death Dis.*, **16**(1): 158.

Du D, Liu C, Qin M, Zhang X, Xi T, Yuan S, Hao H and Xiong J (2022). Metabolic dysregulation and emerging therapeutical targets for hepatocellular carcinoma. *Acta Pharm. Sin. B.*, **12**(2): 558-580.

Giannone G, Ghisoni E, Genta S, Scotto G, Tuninetti V, Turinetto M and Valabrega G (2020). Immuno-metabolism and microenvironment in cancer: Key players for immunotherapy. *Int. J. Mol. Sci.*, **21**(12): 4414.

Harding-Theobald E, Louissaint J, Maraj B, Cuaresma E, Townsend W, Mendiratta-Lala M, Singal AG, Su GL, Lok AS and Parikh ND (2021). Systematic review: Radiomics for the diagnosis and prognosis of hepatocellular carcinoma. *Aliment. Pharmacol. Ther.*, **54**(7): 890-901.

Huang A, Yang XR, Chung WY, Dennison AR and Zhou J (2020). Targeted therapy for hepatocellular carcinoma. *Signal Transduct Target Ther.*, **5**(1): 146.

Huo J, Wu L and Zang Y (2021). Development and validation of a CTNNB1-associated metabolic prognostic model for hepatocellular carcinoma. *J. Cell. Mol. Med.*, **25**(2): 1151-1165.

Jin S, Guerrero-Juarez CF, Zhang L, Chang I, Ramos R, Kuan CH, Myung P, Plikus MV and Nie Q (2021). Inference and analysis of cell-cell communication using CellChat. *Nat. Commun.*, **12**(1): 1088.

Liberzon A, Birger C, Thorvaldsdóttir H, Ghandi M, Mesirov JP and Tamayo P (2015). The molecular signatures database (MSigDB) hallmark gene set collection. *Cell Syst.*, **1**(6): 417-425.

Li T, Fu J, Zeng Z, Cohen D, Li J, Chen Q, Li B and Liu XS (2020). TIMER2.0 for analysis of tumor-infiltrating immune cells. *Nucleic Acids Res.*, **48**(W1): W509-W514.

Liu Y, Song J, Shi Q, Chen B, Qiu W, Liu Y, Huang S and He X (2024). Glucose-induced LINC01419 reprograms the glycolytic pathway by recruiting YBX1 to enhance PDK1 mRNA stability in hepatocellular carcinoma. *Clin. Transl. Med.*, **14**(12): e70122.

Llibre A, Kucuk S, Gope A, Certo M and Mauro C (2025). Lactate: A key regulator of the immune response. *Immunity*, **58**(3): 535-554.

Long J, Wang A, Bai Y, Lin J, Yang X, Wang D, Yang X, Jiang Y and Zhao H (2019). Development and validation of a TP53-associated immune prognostic model for hepatocellular carcinoma. *EBioMedicine*, **42**: 363-374.

Lu C, Rong D, Zhang B, Zheng W, Wang X, Chen Z and Tang W (2019). Current perspectives on the immunosuppressive tumor microenvironment in hepatocellular carcinoma: Challenges and opportunities. *Mol. Cancer*, **18**(1): 130.

Nguyen NTB, Gevers S, Kok RNU, Burgering LM, Neikes H, Akkerman N, Betjes MA, Ludikhuize MC, Gulersonmez C, Stigter ECA, Vercoulen Y, Drost J, Clevers H, Vermeulen M, van Zon JS, Tans SJ, Burgering BMT and Rodriguez MJ (2025). Lactate controls cancer stemness and plasticity through epigenetic regulation. *Cell Metab.*, **37**(4): 903-919, e10.

Oura K, Morishita A, Tani J and Masaki T (2021). Tumor immune microenvironment and immunosuppressive therapy in hepatocellular carcinoma: A review. *Int. J. Mol. Sci.*, **22**(11): 5801.

Pedretti S, Palermo F, Braghin M, Imperato G, Tomaiuolo P, Celikag M, Boccazzi M, Vallelonga V, Da Dalt L, Norata GD, Marisi G, Rapposelli IG, Casadei-Gardini A, Ghisletti S, Crestani M, De Fabiani E and Mitro N (2025). D-lactate and glycerol as potential biomarkers of sorafenib activity in hepatocellular carcinoma. *Signal Transduct Target Ther.*, **10**(1): 200.

Rabinowitz JD and Enerback S (2020). Lactate: The ugly duckling of energy metabolism. *Nat. Metab.*, **2**(7): 566-571.

Sartoris R, Gregory J, Dioguardi Burgio M, Ronot M and Vilgrain V (2021). HCC advances in diagnosis and prognosis: Digital and Imaging. *Liver Int.*, **41**(Suppl 1): 73-77.

Sheng H, Huang Y, Xiao Y, Zhu Z, Shen M, Zhou P, Guo Z, Wang J, Wang H, Dai W, Zhang W, Sun J and Cao C (2020). ATR inhibitor AZD6738 enhances the antitumor activity of radiotherapy and immune checkpoint inhibitors by potentiating the tumor immune microenvironment in hepatocellular carcinoma. *J. Immunother. Cancer*, **8**(1): e000340.

Tang B, Zhu J, Li J, Fan K, Gao Y, Cheng S, Kong C, Zheng L, Wu F, Weng Q, Lu C and Ji J (2020). The ferroptosis and iron-metabolism signature robustly predicts clinical diagnosis, prognosis and immune microenvironment for hepatocellular carcinoma. *Cell Commun. Signal*, **18**(1): 174.

Trapnell C, Cacchiarelli D, Grimsby J, Pokharel P, Li S, Morse M, Lennon NJ, Livak KJ, Mikkelsen TS and Rinn JL (2014). The dynamics and regulators of cell fate decisions are revealed by pseudotemporal ordering of single cells. *Nat. Biotechnol.*, **32**(4): 381-386.

Uhlén M, Fagerberg L, Hallstrom BM, Lindskog C, Oksvold P, Mardinoglu A, Sivertsson A, Kampf C, Sjöstedt E, Asplund A, Olsson I, Edlund K, Lundberg E, Navani S, Szigyarto CA, Odeberg J, Djureinovic D, Takanen JO, Hober S, Alm T, Edqvist PH, Berling H, Tegel H, Mulder J, Rockberg J, Nilsson P, Schwenk JM, Hamsten M, von Feilitzen K, Forsberg M, Persson L, Johansson F, Zwahlen M, von Heijne G, Nielsen J and Pontén F (2015). Tissue-based map of the human proteome. *Science*, **347**(6220): 1260419.

Wang N, Tan HY, Lu Y, Chan YT, Wang D, Guo W, Xu Y, Zhang C, Chen F, Tang G and Feng Y (2021). PIWIL1 governs the crosstalk of cancer cell metabolism and immunosuppressive microenvironment in

hepatocellular carcinoma. *Signal Transduct Target Ther.*, **6**(1): 86.

Wang W and Wei C (2020). Advances in the early diagnosis of hepatocellular carcinoma. *Genes Dis.*, **7**(3): 308-319.

Wilkerson MD and Hayes DN (2010). Consensus ClusterPlus: A class discovery tool with confidence assessments and item tracking. *Bioinform.*, **26**(12): 1572-1573.

Xia C, Dong X, Li H, Cao M, Sun D, He S, Yang F, Yan X, Zhang S, Li N and Chen W (2022). Cancer statistics in China and United States, 2022: Profiles, trends and determinants. *Chin. Med. J. (Engl.)*, **135**(5): 584-590.

Xu F, Jin T, Zhu Y and Dai C (2018). Immune checkpoint therapy in liver cancer. *J. Exp. Clin. Cancer Res*., **37**(1): 110.

Yeh H, Chiang CC and Yen TH (2021). Hepatocellular carcinoma in patients with renal dysfunction: Pathophysiology, prognosis and treatment challenges. *World J. Gastroenterol*., **27**(26): 4104-4142.

Yeo YH, Abdelmalek M, Khan S, Moylan CA, Rodriquez L, Villanueva A and Yang JD (2025). Current and emerging strategies for the prevention of hepatocellular carcinoma. *Nat. Rev. Gastroenterol. Hepatol*., **22**(3): 173-190.

Yu G, Wang LG, Han Y and He QY (2012). ClusterProfiler: An R package for comparing biological themes among gene clusters. *OMICS*, **16**(5): 284-287.

Zhang Y and Zhang X (2024). Virus-induced histone lactylation promotes virus infection in crustacean. *Adv Sci. (Weinh.)*, **11**(30): e2401017.

Zheng J, Wang S, Xia L, Sun Z, Chan KM, Bernards R, Qin W, Chen J, Xia Q and Jin H (2025). Hepatocellular carcinoma: Signaling pathways and therapeutic advances. *Signal Transduct Target Ther*., **10**(1): 35.

Ziogas A, Novakovic B, Ventriglia L, Galang N, Tran KA, Li W, Matzaraki V, van Unen N, Schluter T, Ferreira AV, Moorlag S, Koeken V, Moyo M, Li X, Baltissen MPA, Martens JHA, Li Y, Divangahi M, Joosten LAB, Mhlanga MM and Netea MG (2025). Long-term histone lactylation connects metabolic and epigenetic rewiring in innate immune memory. *Cell*, **188**(11): 2992-3012, e16.